Chemical Physics Letters 758 (2020) 137905

Contents lists available at ScienceDirect

Chemical Physics Letters

journal homepage: www.elsevier.com/locate/cplett

Research paper

Photo-induced electron transfer between a metal nanoparticle and a collection of molecular emitters

Junais Habeeb Mokkath

Quantum Nanophotonics Simulations Lab, Department of Physics, Kuwait College of Science And Technology, 7th Ring Road, P.O. Box 27235, Doha Area, Kuwait

HIGHLIGHTS

- We investigate hybrid polaritonic nanostructures using the TD-DFT technique.
- We found a strong coupling between the plasmonic nanoparticle and molecular emitter states.
- Our finding useful for the development of novel hybrid polaritonic nanostructures.

ARTICLE INFO

Keywords:
TD-DFT
Plasmons
Excitons

ABSTRACT

Hybrid polaritonic nanostructures combining molecular excitons and localized surface plasmons hold strong potential for promising applications in broad areas of nanophotonics. Here, using quantum mechanical calculations, we study the position- and configuration-dependent optical response modulations in a hybrid system composed of a plasmonic nanoparticle and a collection of molecular emitters. Our results underline the coupling between the plasmonic nanoparticle and molecular emitter states, confirmed from the transition density maps. Depending on the interparticle distance (d) and the number of coupled molecular emitters, we show that photo-induced electron transfer emerge. Our theoretical findings bear fundamental interest for the development of novel hybrid polaritonic nanostructures.

1. Introduction

Designer polaritonic nanostructures such as the metal nanoparticle (MNP) in combination with the molecular emitters (MEs) is of paramount importance for the high-end emerging applications in nanophotonics [1–10]. Polaritonic nanostructures couple resonantly matched localized surface plasmons (collective motion of the metallic electrons) of MNP and excitons (electron-hole pairs) of MEs. Understanding the nature and tunability of polaritonic states are important and triggered the vast range of possible applications in areas as diverse as chemical sensors [11], pH meters [12], and light harvesters [13], to list a few. Bringing a ME near to an MNP results in the hybridization of the discrete states of the former and the continuum-like states of the latter [14–26]. Besides, polaritonic structures trigger resonant electron transfer between the individual building blocks. In general, increased interactions between MEs and MNPs should ultimately lead to strongly hybridized polaritonic states with characteristics largely distinct from either the ME or MNP properties alone.

Thanks to the advanced nanofabrication techniques developed recently allowing the engineer novel polaritonic nanostructures with nanometer control of their geometry. On the theoretical side, this technological progresses poses new challenges since conventional classical electrodynamics approaches such as discrete-dipole approximation [27], finite-difference time domain techniques [28], T-matrix [29], boundary element method [30], and plasmon hybridization formalism [31] might not be adequate to describe completely the hybridization between MEs and MNP and thus need to be applied with care. A potential way to tackle this problem is to employ a fully quantum mechanical framework such as the Time Dependent Density Functional Theory (TD-DFT) [32–35]. It is a parameter-free framework (as far as the potential acting on the valence electrons is set) that can properly address the modification of the optical response due to the quantum mechanical effects straightforwardly and accurately. In fact, analytical and numerical quantum chemistry approaches, including DFT and TD-DFT, have been successfully applied to study ME-MNP interactions, charge transfer, and chemical enhancement [36–45]. TD-DFT has been implemented in both the frequency and time domain. TD-DFT in the linear-response regime (*lr*-TDDFT) is often formulated in frequency space [46] in terms of the Casida matrix expressed in the Kohn-Sham electron-hole space [47–49]. The second method, the real-

E-mail address: j.mokath@kcst.edu.kw.

https://doi.org/10.1016/j.cplett.2020.137905
Received 21 July 2020; Received in revised form 17 August 2020; Accepted 18 August 2020
Available online 26 August 2020

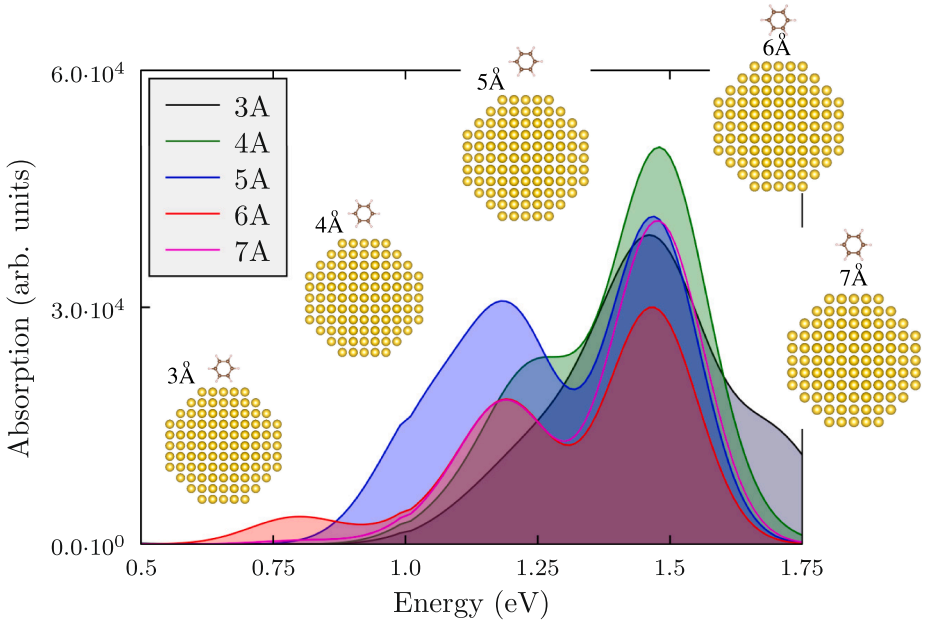

Fig. 1. TD-DFT calculated photo-absorption spectra (averaged over all directions of light polarization) of group1 hybrids. Note that *d* vary in the range of 3–7 Å.

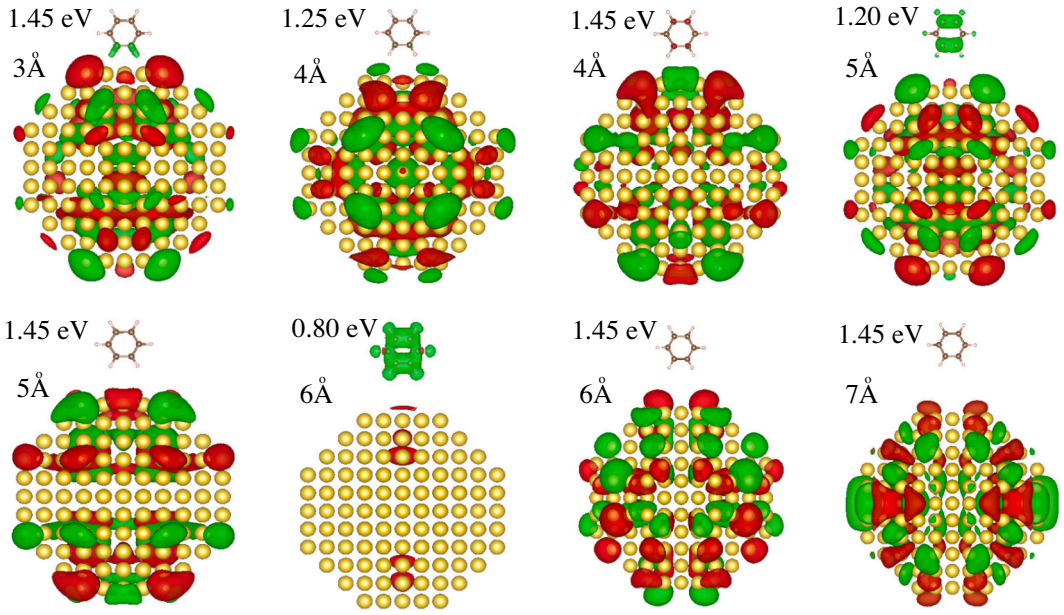

Fig. 2. Transition density map corresponding to some representative peaks of group1 hybrids. Green (red) color shows positive (negative) transition charge densities. Both densities are plotted using the same iso-surface contour value. (For interpretation of the references to color in this figure legend, the reader is referred to the web version of this article.)

time-propagation formulation of TD-DFT (*rt*-TDDFT) is based on integrating the time-dependent Kohn-Sham equations in time [50–52]. While *lr*-TDDFT is limited to the weak perturbation field to meet the requirement of the linear-response approximation, *rt*-TDDFT allows one to capture the effects of external fields both in the weak and strong interaction regimes [53,54].

In this Article, we theoretically investigate the nature and tunability of photo-induced resonant electron transfer between a single and/or a collection of MEs and an MNP. To that end, we chose benzene molecule as ME and a spherical sodium nanoparticle as MNP. In particular, we reveal scenarios in which the coupling of the MEs with the MNP emerges for a broad range of distances. When a ME is located in the tunneling regime, the situation becomes even more complex, and the effect of electron tunneling involving the ME localized states can strongly affect the response of the whole hybrid system. As a key result of our paper, we show that the investigated systems reveal photo-induced resonant electron transfers. We reached this conclusion by analysing the transition density maps (TDMs): a generalization of the transition dipole moment describing the transition between the Nth excited state and ground state [55,56]. In fact, we are not aware of a fully quantum mechanical study on the polaritonic systems investigated in this work and more importantly, the critical question of the influence of the photo-induced electron transfer on the number of MEs and *d* values are remain elusive. The present work aims at answering these questions using TD-DFT calculations. We hope that the results of this study will contribute to the improvement of our understanding of the photo-induced resonant electron transfer between ME and MNP. We have organized this paper as follows. First, we describe the systems

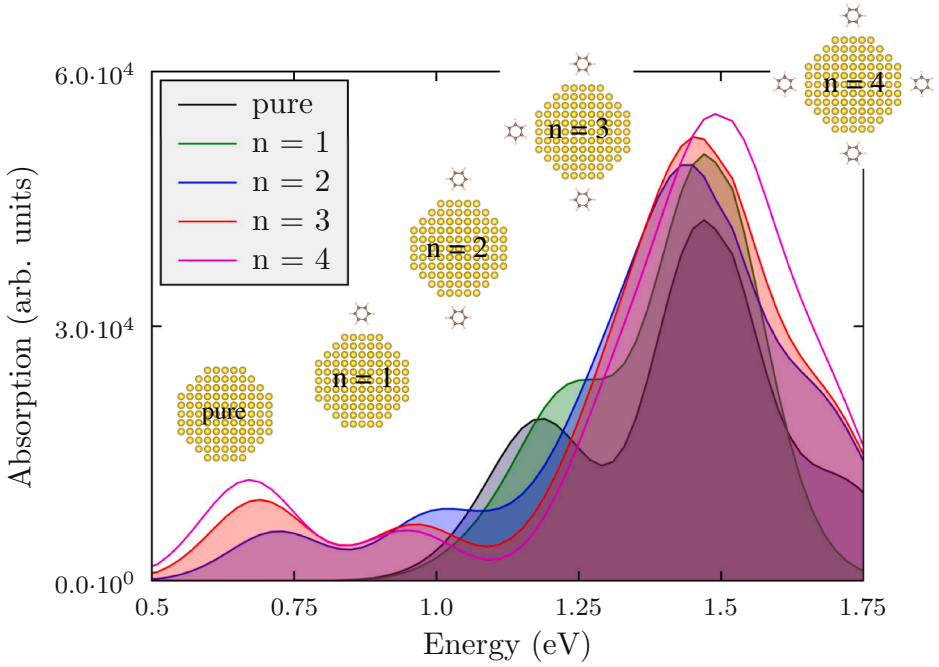

Fig. 3. TD-DFT calculated photo-absorption spectra (averaged over all directions of light polarization) of group2 hybrids with d = 4 Å. n represents the number of benzene molecules.

under study and the simulations methods employed. We show our results and discuss them in the next section, addressing the optical absorption spectra and the transition density maps. The conclusions and outlook section closes the paper.

2. Methodology

DFT/TD-DFT calculations in this study were carried out using the ORCA software (version 4.0) [57] with the LANL2DZ effective core potential basis set [58] and B3-LYP exchange-correlation functional [59]. We consider a proof-of-principle system based on a spherical Na nanoparticle. The free-electron-like electronic structure of Na greatly simplifies the analysis in contrast to noble metals with d electron-screened plasmons. Our model systems consist of a Na nanoparticle (regular truncated octahedra with 369 atoms and an approximate diameter of 2.0 nm) and benzene molecules. We chose Na nanoparticle due to its prevalence in the literature as a convenient model plasmonic system. Whereas, the selection of benzene molecule is based on its ability to modify the plasmonic field produced by the nearby nanoparticle. Details of the DFT/TD-DFT simulations employed here can be found elsewhere [57]. Retardation effects are neglected due to the small size of the system. Below we describe only the main aspects important for the present study. In the first step, we performed DFT structural relaxation of the individual components (benzene molecule and Na nanoparticle) subjected to strict convergence conditions: SCF convergence: 10^{-8}, gradient convergence: 10^{-6}, and energy convergence: 10^{-6}. In the next step, using the individual (optimized) systems, we modeled two kinds of hybrids. The group1 hybrid is composed of a benzene molecule coupled to a Na nanoparticle (the benzene molecule placed at one of the {1 0 0} facet) with d vary in the range of 3–7 Å, see Fig. 1. The selection of d is based on the coupling strength between the Na nanoparticle and benzene molecule. More specifically, d = 3 Å rendered the maximum coupling strength (strong coupling regime), whereas, for d = 7 Å, the coupling strength reduced to 20%. The group2 hybrid is composed of benzene molecules (their number varies from two to four) placed at the {100} facets of a Na nanoparticle with d vary in the range of 4–6 Å, see Fig. 3. Structural relaxation of hybrids is neglected for simplicity since we wanted to preclude the influence of geometrical effects (i.e., small variations in the inter-atomic distances) on the optical features. It should be mentioned that the calculated lowest energy structures of hybrids are arranged in such a way that the benzene molecule is oriented perpendicular to the NP surface. This result is in tune with the low-temperature scanning tunnelling microscopy and Raman scattering experiments where pyridine binds to the Ag NP through the nitrogen atom [60]. The calculated binding energies in the present study for Na nano-particle with benzene oriented parallel and perpendicular to the surface are 3.50 and 4.25 eV, respectively. We computed the optical absorption spectra using *lr*-TDDFT technique. We solved Casida eigenvalue equation $\Omega F_I = \omega_I^2 F_I$, where Ω is a matrix consisting of products of occupied-virtual Kohn-Sham orbitals and the eigenvalues ω_I^2 correspond to squared excitation energies while the oscillator strengths are extracted from the eigenvectors F_I [61]. The number of dipole-allowed transitions has to be set to a high number in order to obtain an absorption spectrum in the desired energy range. For example, 110 transitions are required to compute the absorption spectrum of the group2 hybrid in the spectral range of 0 eV to 1.75 eV. All absorption spectra are broadened by Gaussian smearing of width σ = 0.10 eV. The main peaks appearing in the optical absorption spectra are analyzed using transition density plots. The incorporation of long-range correction resulted in a slight reduction in the absorption peak intensities while retaining the gross shape of the absorption profile and the absorption onset. We remark that the used exchange-correlation functional (B3-LYP) is sufficient for the purposes of the present work.

3. Results and discussion

We first study the optical absorption spectra of group1 hybrids (a benzene molecule coupled to a Na nanoparticle) as shown in Fig. 1. A first conclusion from Fig. 1 is that the systems display dramatic optical response modulations with the d value in the range of 3–7 Å. In particular, notable differences become apparent in the absorption onset. For d in the range of 3–6 Å, one sees systematic red-shifts in the absorption onset. However, the situation changes in the case of d = 7 Å where one finds blue-shift of the absorption onset. Nevertheless, Fig. 1 demonstrates that the spectral evolution as a function of d can be effectively classified into three interaction regimes. For small d values of 3 and 4 Å, notable differences become apparent as the chemical bonding between the ME and MNP emerges. For d = 5 and 6 Å, the quantum tunneling does substantially impact the response of the system. In particular, one sees the emergence of absorption in the low-

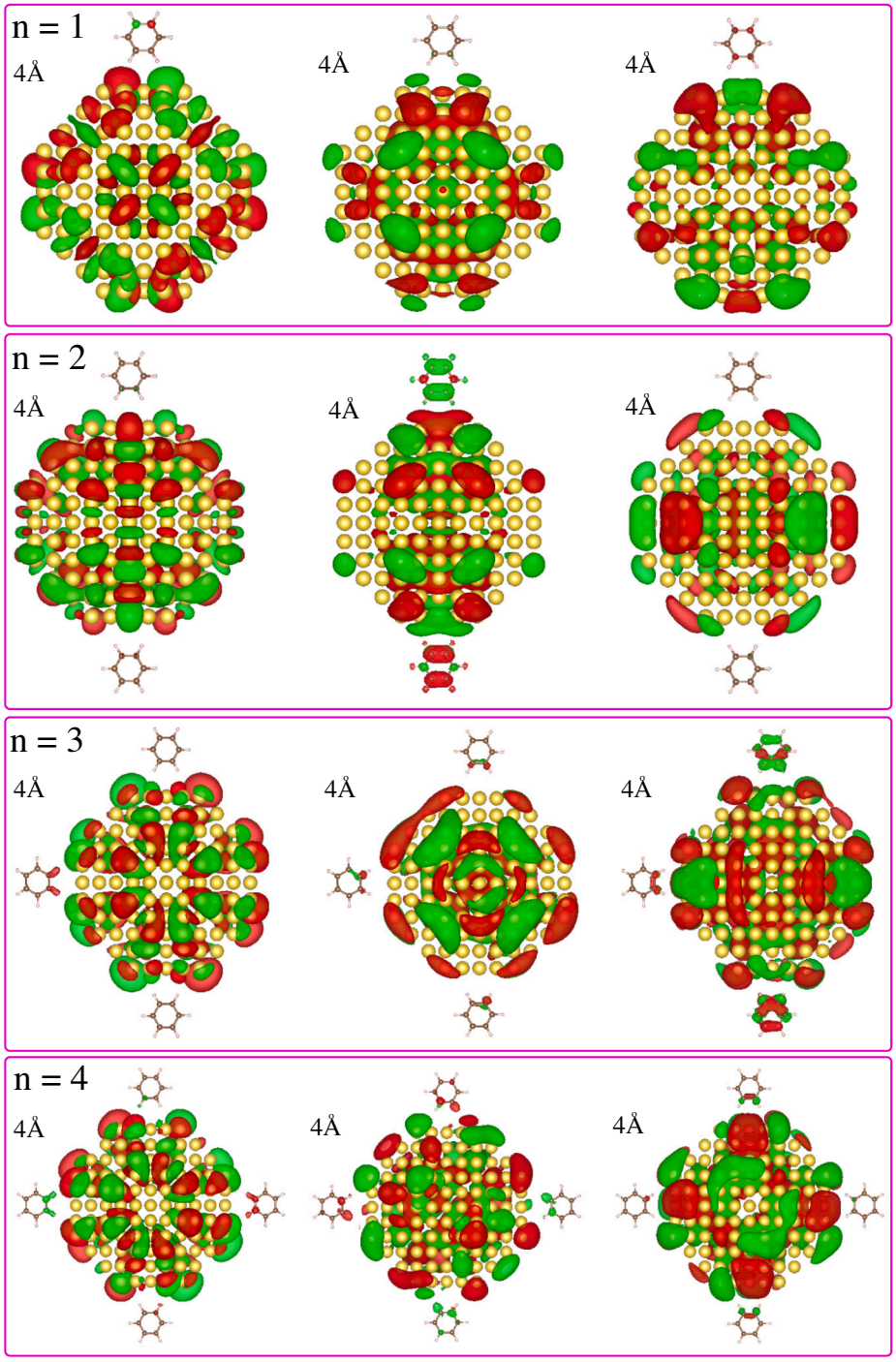

Fig. 4. Transition density map corresponding to some representative peaks of group2 hybrids with $d = 4$ Å. n represents the number of benzene molecules. Green (red) color shows positive (negative) transition charge densities. Both densities are plotted using the same iso-surface contour value. (For interpretation of the references to color in this figure legend, the reader is referred to the web version of this article.)

energy region provide a strong indication of electron tunneling between subsystems. At larger gap distance of $d = 7$ Å, the ME and MNP are chemically and physically separated. Now we analyse in detail the spectral modulations for each d values separately. For the smallest d value of 3 Å, the absorption spectrum is primarily composed of a single prominent peak centered around 1.45 eV. It should be emphasized that this dominant peak is composed of several single-particle excitations: HOMO − 2→LUMO + 4 (81%) and HOMO − 3→LUMO + 5 (5%). While moving to $d = 4$ Å, one finds significant absorption intensity enhancements. In particular, the absorption intensity of the prominent peak significantly enhanced. In addition, a new peak appears around 1.25 eV. This peak is composed of a single-particle excitation of HOMO − 2→LUMO + 8 (98%). More dramatic spectral modulations emerge for $d = 5$ Å. One observes a high intensity spectral peak centered around 1.20 eV and at the same time the spectral intensity of the prominent the peak centered around 1.45 eV significantly reduced. Further spectral modulations appear in the case of $d = 6$ Å. One finds that the 1.20 eV peak reduced its absorption intensity by causing a new peak to appear, which is centered around 0.80 eV. This peak is composed of 3 single-particle excitations mainly consisting of HOMO − 2→LUMO + 4 (92%) and HOMO − 2→LUMO + 2 (5%). Finally, in the case of $d = 7$ Å, the peak centered around 0.80 eV eventually disappeared.

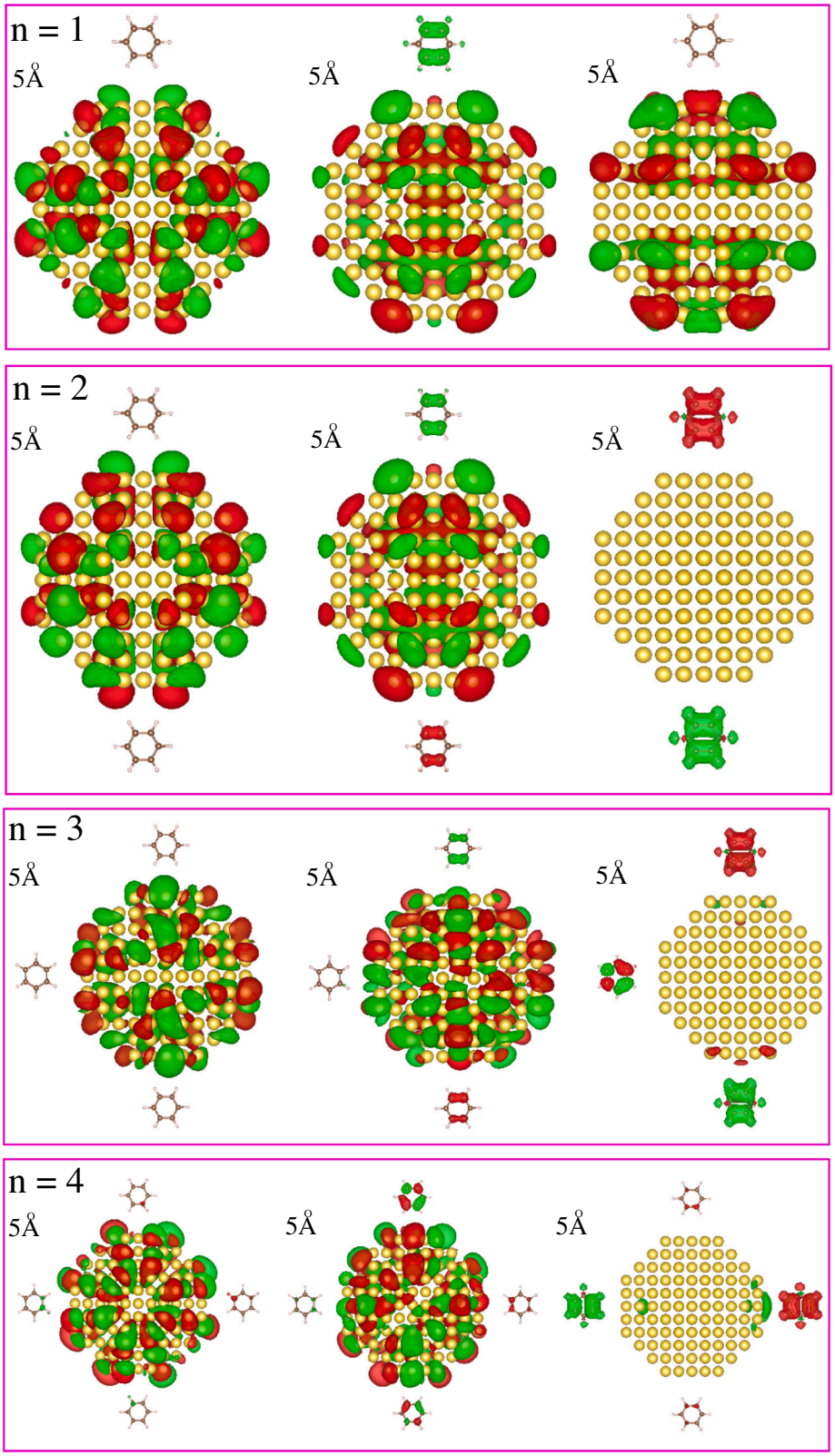

Fig. 5. Transition density map corresponding to some representative peaks of group2 hybrids with $d = 5$ Å. n represents the number of benzene molecules. Green (red) color shows positive (negative) transition charge densities. Both densities are plotted using the same iso-surface contour value. (For interpretation of the references to color in this figure legend, the reader is referred to the web version of this article.)

Additionally, the prominent peak centered around 1.45 eV gained pronounced absorption intensity. Having analyzed/discussed the optical absorption spectra of a single benzene molecule attached to a Na nanoparticle, we now focus our attention on transition density maps (TDMs), see Fig. 2. TDMs provide beneficial information regarding the microscopic origin of the absorption peaks, which is representative of the spatial localization of the electron excitations. Nevertheless, one key observation from Fig. 2 is that for $d = 6$ Å (for peak centered

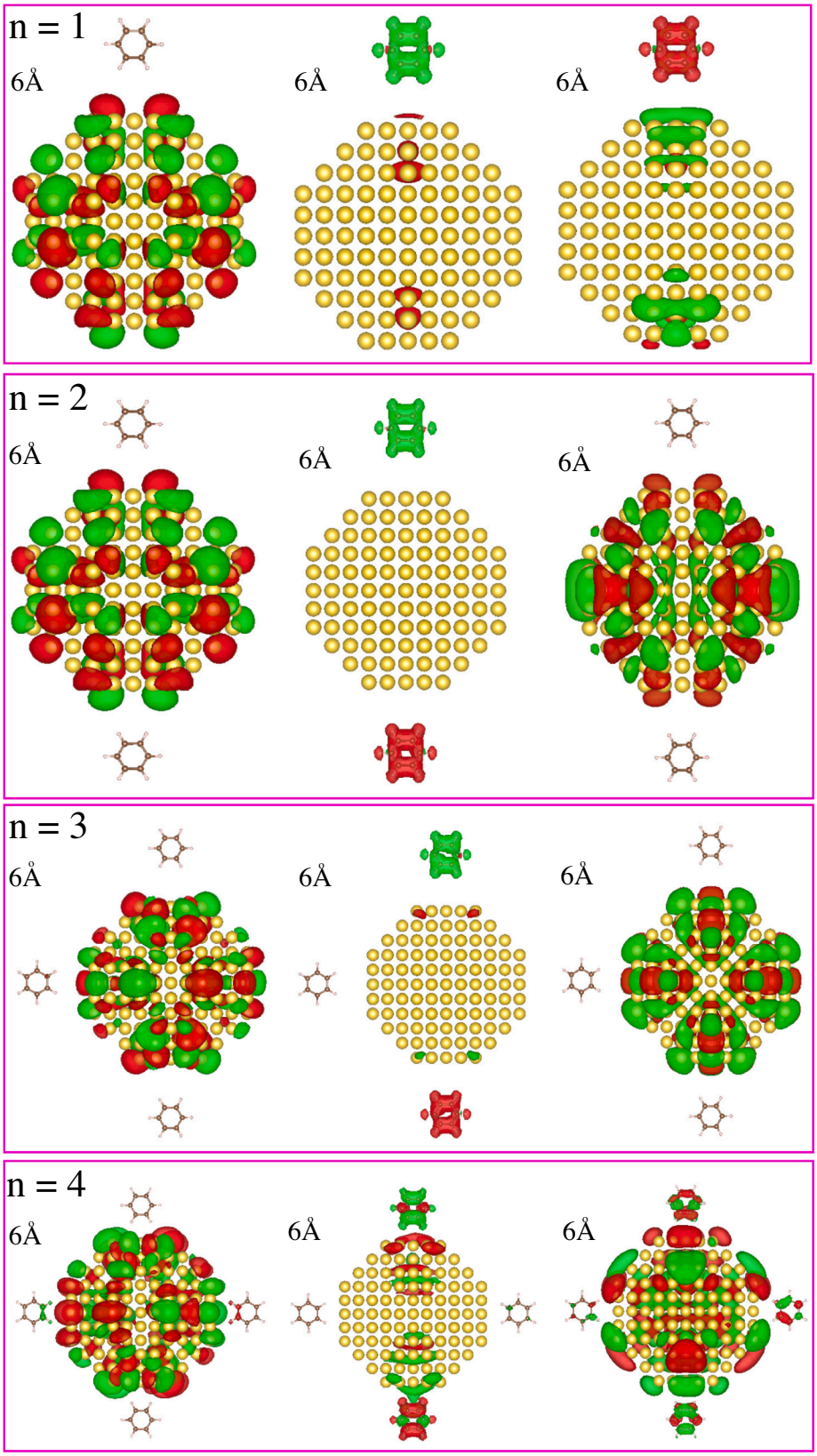

Fig. 6. Transition density map corresponding to some representative peaks of group2 hybrids with $d = 6$ Å. n represents the number of benzene molecules. Green (red) color shows positive (negative) transition charge densities. Both densities are plotted using the same iso-surface contour value. (For interpretation of the references to color in this figure legend, the reader is referred to the web version of this article.)

around 0.80 eV), the positive (green) and negative (red) transition charge densities are mostly focused at the benzene molecule and Na nanoparticle, respectively, can primarily be attributed to the photo-induced electron transfer between the two subsystems. In contrast, the rest of the TDM plots in Fig. 2 demonstrate that both the positive and negative transition charge densities are distributed over the entire extent of the benzene molecule and/or Na nanoparticle.

Having analyzed/discussed the optical absorption spectra and transition density maps of the group1 hybrids (benzene molecule coupled to a Na nanoparticle), next, we study the group2 hybrids consist of benzene molecules (number n vary from two to four) and a Na nanoparticle with d vary in the range of 4–6 Å. Let us first discuss the characteristic of the spectral evolution starting from $d = 4$ Å, see Fig. 3. Notice that for $n = 2$, 3, and 4, a low-energy peak (in the spectral range between 0.50 eV and 0.75 eV) starts to emerge having monotonously increasing its absorption intensity. This is an interesting result since it simply shows that the key effect of adding benzene molecules on the nanoparticle surface is to create a low-energy peak (as a result of the benzene molecules and Na nanoparticle interaction). Concurrently, the absorption intensity of the low-energy peak increases with the increasing number of the benzene molecules. Now let us analyse/discuss in detail the spectral modulations for the increasing number (n) of benzene molecules. Specifically, for $n = 2$, there appears two low-energy peaks (the first peak centered around 0.70 eV: composed of single-particle excitation HOMO→LUMO + 15 (98%) and second peak centered around 1.0 eV: composed of single-particle excitation HOMO − 1LUMO + 4 (100%)) and a prominent peak centered around 1.40 eV. In the case of $n = 3$, Fig. 3 shows that both the low-energy peak (centered around 0.70 eV and 1.0 eV) further red-shifts. Apparently, this result indicates that increasing the number of molecules coupled to the Na nanoparticle cause increased interaction between the subsystems. Remarkably, for $n = 4$, the low-energy peak further red-shifted to 0.60 eV: it is composed of 3 single-particle excitations mainly consisting of HOMO→LUMO + 14 (84%), HOMO→LUMO + 17 (12%), and HOMO→LUMO + 15 (1%) and the high-energy dominant peak considerably gained in the spectral intensity. Clearly, $n = 4$ records the maximum spectral intensity in comparison to all other n values. Now let us analyze the transition density maps corresponding to the peaks as mentioned earlier, see Fig. 4. It is noteworthy that for $n = 2$, the transition density map located in the middle position presents an unusual transition density distribution. This is readily visible since the transition density of the Na nanoparticle is symmetrically distributed while transition densities of the benzene molecules are distributed with opposite polarities. Alternatively, while coming to the case of $n = 3$, one sees the transition charge densities are almost symmetrically distributed for the first two excitations, whereas, mixed excitations involving both the benzene molecules and Na nanoparticle emerge in the case of the last excitation. Likewise, in the case of $n = 4$, one observes a highly symmetric distribution of transition densities reflecting the symmetry of the underlying system. Incidentally, we also remark that our results may impact a variety of fields in nano-optics dealing with localized states in the proximity of plasmonic nanoparticles, such as in sensing and photo-chemical processes.

Having analyzed/discussed the differences and similarities in the distribution of the transition densities corresponding to $d = 4$ Å, we briefly analyze the transition density maps (to discern the specific nature of the optical excitations) corresponding to $d = 5$ and 6 Å, see Fig. 5 and Fig. 6, respectively. One finds interesting results from Fig. 5. In particular, the last transition density plot for $n = 2$. One finds no transition density distribution on Na nanoparticle, however, benzene molecules hold both the positive and negative transition densities. Similar results can also be observed in the case of $n = 3$ and 4. Likewise, we briefly discuss the transition density plots corresponding to $d = 6$ Å. One observes a different variety of transition density maps. For example, some excitations are fully localized to the benzene molecules (middle excitation of $n = 2$) or some excitations fully localized to Na nanoparticle (first excitation of $n = 3$) and some mixed type excitations (third excitation of $n = 4$) involving both the benzene molecules and Na nanoparticle. Some comments are in order regarding the generality of the results. Despite present calculations that have been performed with benzene molecules and Na nanoparticle, the qualitative results are robust and are caused by universal quantum mechanical phenomena such as electron tunneling.

4. Conclusions

Coupling molecular excitations and localized surface plasmon resonances of hybrid nanosystems is an exciting field to explore novel optical properties. Moreover, it is a widely acknowledged fact that the strong and localized field in a plasmonic hotspot enhances the interaction between localized surface plasmon resonances and the molecular excitations. To this end, we conducted quantum mechanical calculations, elucidating the optical properties of hybrid nanosystems consists of benzene molecules coupled to a Na nanoparticle. We seek understanding of our results using the transition density maps. This helped us to differentiate the nature of the optical excitation. As a main conclusion of our work, depending on gap separation distances and number of molecular emitters, photo-induced electron transfer emerge. We believe that the results obtained in this study can be useful in cavity induced photo-catalysis.

CRediT authorship contribution statement

Junais Habeeb Mokkath: Conceptualization, Methodology, Software, Validation, Writing - original draft.

Declaration of Competing Interest

The authors declare that they have no known competing financial interests or personal relationships that could have appeared to influence the work reported in this paper.

Acknowledgement

The research reported in this publication was supported by funding from Kuwait College of Science And Technology (KCST).

Appendix A. Supplementary material

Supplementary data associated with this article can be found, in the online version, at https://doi.org/10.1016/j.cplett.2020.137905.

References

[1] P. Törmä, W.L. Barnes, Strong coupling between surface plasmon polaritons and emitters: a review, Rep. Prog. Phys. 78 (2014) 013901.
[2] D.G. Baranov, M. Wersäll, J. Cuadra, T.J. Antosiewicz, T. Shegai, Novel nanostructures and materials for strong light-matter interactions, ACS Photonics 5 (2018) 24–42.
[3] A. Manjavacas, F.J. García de Abajo, P. Nordlander, Quantum plexcitonics: strongly interacting plasmons and excitons, Nano Lett. 11 (2011) 2318–2323 PMID: 21534592.
[4] A.E. Schlather, N. Large, A.S. Urban, P. Nordlander, N.J. Halas, Near-field mediated plexcitonic coupling and giant rabi splitting in individual metallic dimers, Nano Lett. 13 (2013) 3281–3286 PMID: 23746061.
[5] O. Pérez-González, N. Zabala, J. Aizpurua, Optical properties and sensing in plexcitonic nanocavities: from simple molecular linkers to molecular aggregate layers, Nanotechnology 25 (2013) 035201.
[6] D.C. Marinica, H. Lourenço-Martins, J. Aizpurua, A.G. Borisov, Plexciton quenching by resonant electron transfer from quantum emitter to metallic nanoantenna, Nano Lett. 13 (2013) 5972–5978 PMID: 24206447.
[7] N.T. Fofang, N.K. Grady, Z. Fan, A.O. Govorov, N.J. Halas, Plexciton dynamics: exciton-plasmon coupling in a J-aggregate-Au nanoshell complex provides a mechanism for nonlinearity, Nano Lett. 11 (2011) 1556–1560 PMID: 21417362.
[8] R. Chikkaraddy, B. de Nijs, F. Benz, S.J. Barrow, O.A. Scherman, E. Rosta, A. Demetriadou, P. Fox, O. Hess, J.J. Baumberg, Single-molecule strong coupling at room temperature in plasmonic nanocavities, Nature 535 (2016) 127 EP –.

[9] G.A. Wurtz, P.R. Evans, W. Hendren, R. Atkinson, W. Dickson, R.J. Pollard, A.V. Zayats, W. Harrison, C. Bower, Molecular plasmonics with tunable exciton-plasmon coupling strength in J-aggregate hybridized au nanorod assemblies, Nano Lett. 7 (2007) 1297–1303 PMID: 17455984.

[10] T. Neuman, R. Esteban, D. Casanova, F.J. García-Vidal, J. Aizpurua, Coupling of molecular emitters and plasmonic cavities beyond the point-dipole approximation, Nano Lett. 18 (2018) 2358–2364 PMID: 29522686.

[11] C.J. Murphy, Peer reviewed: optical sensing with quantum dots, Analyt. Chem. 74 (2002) 520 A–526 A.

[12] S.W. Bishnoi, C.J. Rozell, C.S. Levin, M.K. Gheith, B.R. Johnson, D.H. Johnson, N.J. Halas, All-optical nanoscale pH meter, Nano Lett. 6 (2006) 1687–1692 PMID: 16895357.

[13] F. Nan, S.-J. Ding, L. Ma, Z.-Q. Cheng, Y.-T. Zhong, Y.-F. Zhang, Y.-H. Qiu, X. Li, L. Zhou, Q.-Q. Wang, Plasmon resonance energy transfer and plexcitonic solar cell, Nanoscale 8 (2016) 15071–15078.

[14] M. Pelton, J. Aizpurua, G. Bryant, Metal-nanoparticle plasmonics, Laser Photonics Rev. 2 (2008) 136–159.

[15] P. Mühlschlegel, H.-J. Eisler, O.J.F. Martin, B. Hecht, D.W. Pohl, Resonant optical antennas, Science 308 (2005) 1607–1609.

[16] P. Bharadwaj, B. Deutsch, L. Novotny, Optical antennas, Adv. Opt. Photon. 1 (2009) 438–483.

[17] V. Giannini, A.I. Fernández-Domínguez, S.C. Heck, S.A. Maier, Plasmonic nanoantennas: fundamentals and their use in controlling the radiative properties of nanoemitters, Chem. Rev. 111 (2011) 3888–3912 PMID: 21434605.

[18] S.A. Maier, P.G. Kik, H.A. Atwater, S. Meltzer, E. Harel, B.E. Koel, A.A.G. Requicha, Local detection of electromagnetic energy transport below the diffraction limit in metal nanoparticle plasmon waveguides, Nat. Mater. 2 (2003) 229–232.

[19] M. Barbry, P. Koval, F. Marchesin, R. Esteban, A.G. Borisov, J. Aizpurua, D. Sánchez-Portal, Atomistic near-field nanoplasmonics: reaching atomic-scale resolution in nanooptics, Nano Lett. 15 (2015) 3410–3419 PMID: 25915173.

[20] S. Oldenburg, R. Averitt, S. Westcott, N. Halas, Nanoengineering of optical resonances, Chem. Phys. Lett. 288 (1998) 243–247.

[21] H. Xu, E.J. Bjerneld, M. Käll, L. Börjesson, Spectroscopy of single hemoglobin molecules by surface enhanced raman scattering, Phys. Rev. Lett. 83 (1999) 4357–4360.

[22] R. Alvarez-Puebla, L.M. Liz-Marzán, F.J. García de Abajo, Light concentration at the nanometer scale, J. Phys. Chem. Lett. 1 (2010) 2428–2434.

[23] B. Peng, D.B. Lingerfelt, F. Ding, C.M. Aikens, X. Li, Real-time TDDFT studies of exciton decay and transfer in silver nanowire arrays, J. Phys. Chem. C 119 (2015) 6421–6427.

[24] N.V. Ilawe, M.B. Oviedo, B.M. Wong, Real-time quantum dynamics of long-range electronic excitation transfer in plasmonic nanoantennas, J. Chem. Theory Comput. 13 (2017) 3442–3454 PMID: 28679057.

[25] G. Donati, D.B. Lingerfelt, C.M. Aikens, X. Li, Anisotropic polarizability-induced plasmon transfer, J. Phys. Chem. C 122 (2018) 10621–10626.

[26] N.V. Ilawe, M.B. Oviedo, B.M. Wong, Effect of quantum tunneling on the efficiency of excitation energy transfer in plasmonic nanoparticle chain waveguides, J. Mater. Chem. C 6 (2018) 5857–5864.

[27] E.M. Purcell, C.R. Pennypacker, Scattering and absorption of light by nonspherical dielectric grains, Astrophys. J. 186 (1973) 705–714.

[28] A. Taflove, S.C. Hagness, Computational electrodynamics : the finite-difference time-domain method, Artech House (2005).

[29] N.G. Khlebtsov, T-matrix method in plasmonics: An overview, J. Quant. Spectrosc. Radiative Transf. 123 (2013) 184–217 (Peter C. Waterman and his scientific legacy).

[30] V. Myroshnychenko, E. Carbó-Argibay, I. Pastoriza-Santos, J. Pérez-Juste, L.M. Liz-Marzán, F.J.G. de Abajo, Modeling the optical response of highly faceted metal nanoparticles with a fully 3D boundary element method, Adv. Mater. 20 (2008) 4288–4293.

[31] P. Nordlander, C. Oubre, E. Prodan, K. Li, M.I. Stockman, Plasmon hybridization in nanoparticle dimers, Nano Lett. 4 (2004) 899–903.

[32] M. Marques, E. Gross, Time-dependent density functional theory, Annu. Rev. Phys. Chem. 55 (2004) 427–455 PMID: 15117259.

[33] R.E. Stratmann, G.E. Scuseria, M.J. Frisch, An efficient implementation of time-dependent density-functional theory for the calculation of excitation energies of large molecules, J. Chem. Phys. 109 (1998) 8218–8224.

[34] E. Runge, E.K.U. Gross, Density-functional theory for time-dependent systems, Phys. Rev. Lett. 52 (1984) 997–1000.

[35] J.-L. Calais, Density-functional theory of atoms and molecules. R.G. Parr and W. Yang, Oxford University Press, New York, Oxford, 1989. IX + 333 pp. Price 45.00. International Journal of Quantum Chemistry 1993, 47, 101–101.

[36] P. Vasa, C. Lienau, Strong light-matter interaction in quantum emitter/metal hybrid nanostructures, ACS Photonics 5 (2018) 2–23.

[37] J. Feist, J. Galego, F.J. Garcia-Vidal, Polaritonic chemistry with organic molecules, ACS Photonics 5 (2018) 205–216.

[38] J.F. Arenas, M.S. Woolley, J.C. Otero, J.I. Marcos, Charge-transfer processes in surface-enhanced raman scattering. Franck-Condon active vibrations of pyrazine, J. Phys. Chem. 100 (1996) 3199–3206.

[39] L. Zhao, L. Jensen, G.C. Schatz, Pyridine-Ag20 cluster:? A model system for studying surface-enhanced raman scattering, J. Am. Chem. Soc. 128 (2006) 2911–2919 PMID: 16506770.

[40] J.A. Hutchison, A. Liscio, T. Schwartz, A. Canaguier-Durand, C. Genet, V. Palermo, P. Samorì, T.W. Ebbesen, Tuning the work-function via strong coupling, Adv. Mater. 25 (2013) 2481–2485.

[41] M. Kuisma, A. Sakko, T.P. Rossi, A.H. Larsen, J. Enkovaara, L. Lehtovaara, T.T. Rantala, Localized surface plasmon resonance in silver nanoparticles: Atomistic first-principles time-dependent density-functional theory calculations, Phys. Rev. B 91 (2015) 115431.

[42] S. Malola, L. Lehtovaara, J. Enkovaara, H. Häkkinen, Birth of the localized surface plasmon resonance in monolayer-protected gold nanoclusters, ACS Nano 7 (2013) 10263–10270 PMID: 24107127.

[43] W. Zhu, R. Esteban, A.G. Borisov, J.J. Baumberg, P. Nordlander, H.J. Lezec, J. Aizpurua, K.B. Crozier, Quantum mechanical effects in plasmonic structures with subnanometre gaps, Nat. Commun. 7 (2016) 11495.

[44] P.V. Kumar, T.P. Rossi, M. Kuisma, P. Erhart, D.J. Norris, Direct hot-carrier transfer in plasmonic catalysis, Faraday Discuss. 214 (2019) 189–197.

[45] A. Varas, P. García-González, J. Feist, F. García-Vidal, A. Rubio, Quantum plasmonics: from jellium models to ab initio calculations, Nanophotonics 5 (2016).

[46] C.-P. Hsu, S. Hirata, M. Head-Gordon, Excitation energies from time-dependent density functional theory for linear polyene oligomers? Butadiene to decapentaene, J. Phys. Chem. A 105 (2001) 451–458.

[47] M.E. Casida, Time-dependent density-functional theory for molecules and molecular solids, J. Mol. Struct. THEOCHEM 914 (2009) 3–18 (Time-dependent density-functional theory for molecules and molecular solids).

[48] B. Walker, A.M. Saitta, R. Gebauer, S. Baroni, Efficient approach to time-dependent density-functional perturbation theory for optical spectroscopy, Phys. Rev. Lett. 96 (2006) 113001.

[49] X. Andrade, S. Botti, M.A.L. Marques, A. Rubio, Time-dependent density functional theory scheme for efficient calculations of dynamic (hyper)polarizabilities, J. Chem. Phys. 126 (2007) 184106.

[50] K. Yabana, G.F. Bertsch, Time-dependent local-density approximation in real time, Phys. Rev. B 54 (1996) 4484–4487.

[51] K. Yabana, T. Nakatsukasa, J.-I. Iwata, G.F. Bertsch, Real-time, real-space implementation of the linear response time-dependent density-functional theory, Physica Status Solidi (b) 243 (2006) 1121–1138.

[52] T. Sander, G. Kresse, Macroscopic dielectric function within time-dependent density functional theory–Real time evolution versus the Casida approach, J. Chem. Phys. 146 (2017) 064110.

[53] S. Tussupbayev, N. Govind, K. Lopata, C.J. Cramer, Comparison of real-time and linear-response time-dependent density functional theories for molecular chromophores ranging from sparse to high densities of states, J. Chem. Theory Comput. 11 (2015) 1102–1109 PMID: 26579760.

[54] V. Alejandro, G.-G. Pablo, F. Johannes, F.J., G.-V.; R. Angel, Nanoph 5 (2016) 409, 3.

[55] K.D. Chapkin, L. Bursi, G.J. Stec, A. Lauchner, N.J. Hogan, Y. Cui, P. Nordlander, N.J. Halas, Lifetime dynamics of plasmons in the few-atom limit, Proc. Nat. Acad. Sci. 115 (2018) 9134–9139.

[56] Y. Li, C. Ullrich, Time-dependent transition density matrix, Chem. Phys. 391 (2011) 157–163 (Open problems and new solutions in time dependent density functional theory).

[57] F. Neese, Software update: the ORCA program system, version 4.0. Wiley Interdisciplinary Reviews: Computational Molecular, Science 8 (2018) e1327–n/a, e1327.

[58] W.R. Wadt, P.J. Hay, Ab initio effective core potentials for molecular calculations. Potentials for main group elements Na to Bi, J. Chem. Phys. 82 (1985) 284–298.

[59] A.D. Becke, Density-functional thermochemistry. III. The role of exact exchange, J. Chem. Phys. 98 (1993) 5648–5652.

[60] J.R. Hahn, W. Ho, Imaging and vibrational spectroscopy of single pyridine molecules on Ag(110) using a low-temperature scanning tunneling microscope, J. Chem. Phys. 124 (2006) 204708.

[61] M.E. Casida, C. Jamorski, K.C. Casida, D.R. Salahub, Molecular excitation energies to high-lying bound states from time-dependent density-functional response theory: Characterization and correction of the time-dependent local density approximation ionization threshold, J. Chem. Phys. 108 (1998) 4439–4449.